Determination of Optimal Electrode Positions of a Wearable ECG Monitoring System for Detection of Myocardial Ischemia: A Simulation Study

Axel Loewe[1], Walther HW Schulze[1], Yuan Jiang[1,2], Mathias Wilhelms[1], Olaf Dössel[1]

[1]Institute of Biomedical Engineering, Karlsruhe Institute of Technology (KIT), Karlsruhe, Germany
[2]now at Siemens AG, Erlangen, Germany

Abstract

The early detection of myocardial ischemia is an essential lever for its successful treatment. We investigated an ECG monitoring system with 3 electrodes. Optimal electrode positions are determined using a cellular automaton. The spatially heterogeneous effects of myocardial ischemia were modeled by altering 4 electrophysiological parameters: action potential amplitude and duration, conduction velocity as well as resting membrane voltage. Both, transmural heterogeneity and the influence of the border zone were considered in the simulations on three patient models. The detection of myocardial ischemia is based on ST segment deviation from the physiological case. The signals used to find the best electrode positions comprise ischemic regions with different transmural extents in all 17 AHA segments. We show which ischemic ECGs can be detected given a realistic signal-to-noise ratio, false positive rate and maximum response time of the system.

1. Introduction

Wearable patient monitoring systems may become widely used considering the impact of myocardial ischemia as leading cause of morbidity and mortality. Ischemia due to myocardial infarction (MI) is often invisible even to the standard 12-lead ECG in case of *"electrically silent"* non-ST elevation MIs (NSTEMIs) [1, 2]. Instead of aiming for a complete coverage of ischemic events, this study intends to provide the positioning for a three-electrode monitoring system that is optimized to detect a maximum variety of early-stage MIs.

Ischemia at 10 minutes after onset (phase Ia, stage 2) was simulated in 765 constellations, comprising combinations of 17 AHA segments [3], 3 assumptions on the border zone radius and 5 ischemia radii for 3 patients. To cope with the computational complexity of the study, a cellular automaton (CA) was parameterized to resemble patient-specific simulations carried out with a monodomain reaction-diffusion system.

2. Methods

2.1. Anatomical modeling

To reduce the effect of individual anatomical modeling methods, the study was performed three patient datasets with a large variability. Two patient models were obtained from segmentation of MR images. Resolution was 2.27 x 2.27 x 4 mm^3 (heart), 4 x 4 x 4 mm^3 (thorax) for patient K (male, age 61, posterior and posterolateral infarctions) and 1 x 1 x 1 mm^3 (heart), 1 x 1 x 2 mm^3 (thorax) for patient D (male, age 27, healthy). The anatomical model for patient VM was produced by segmentation of the Visible Man dataset. While the first two models include tissue classes for ventricles, skeletal muscle, fat, blood, lungs, kidneys, liver and spleen (with only patient D having an atrial model and only patient K having a stomach model), the Visible Man dataset distinguishes between 31 tissue classes, with the disadvantage of the imaging data not being taken *in vivo*.

Fiber orientation was introduced for the ventricular myocardium using a rule-based approach [4]. For simulations of cardiac source signals, the anatomical datasets were interpolated to an isotropic voxel size of 0.4 mm (patients VM and D) or 0.5 mm (patient K).

2.2. Electrophysiological modeling

Ischemia simulations were carried out using a cellular automaton. Each cardiac voxel represents a set of myocytes and can be excited by either an external stimulus or by activated adjacent voxels. As soon as a cell becomes activated, a predefined transmembrane voltage (TMV) course is triggered. These TMV courses were extracted from simulations using the monodomain reaction-diffusion system *acCELLerate* [5].

To provide for transmural heterogeneity, a patch with a voxel side-length of 0.1 mm was divided transmurally into three slices (subendocardial, midmyocardial and subepicardial) each representing a fraction of 40% / 20% / 20% [6]. Ten Tusscher's cell model [7] was

incorporated to extract 120 TMV courses across the ventricular wall. Additionally, a whole-heart simulation was carried out for each patient geometry in order to obtain the APD_{90} for every cardiac voxel. Besides the transmural heterogeneities described by ten Tusscher et al. [7], the conductivity g_{Ks} was two times larger at the apex than at the base [6]. With the provided information, it became possible to assign each cardiac voxel an individual action potential (AP) regarding the morphology with respect to its transmural position as well as regarding its APD_{90}. Anisotropic tissue conductivities inside the ventricular wall and the endocardial stimulation profile emulating the conduction system were set according to [6].

2.3. Modeling of myocardial ischemia

Weiss et al. presented modifications to ten Tusscher's model, providing for the three main effects of cardiac ischemia: extracellular hyperkalemia, acidosis and hypoxia [8]. The model comprises transmural heterogeneities as well as the degree of ischemia regarding the location of the myocyte with respect to the site of the occlusion by introducing a so-called zone-factor (ZF) ranging from 0 representing healthy tissue to 1 representing voxels in the central ischemic zone (CIZ). The voxels with a ZF between 0 and 1 form the border zone (BZ).
Our approach was to extract the spatially heterogeneous electrophysiological impact of the biochemical effects described above, using a tissue patch with a voxel side-length of 0.1 mm representing a slice of the ventricular wall. The BZ in that *acCELLerate* simulation was made up of 180 voxels with a linearly increasing ZF. The transmural extent of the patch was 160 voxels with an subendo / mid / subepi distribution of 40% / 20% / 20%, again. The results of the monodomain simulation were used to extract four characteristic electrophysiological parameters describing the impact of myocardial ischemia: resting membrane voltage (RMV), AP amplitude, APD_{90} and conduction velocity. These parameters were then used to modulate the TMV courses for the CA with respect to the ZF and the transmural position of the activated voxel.
The ischemia implementation for the CA was validated by calculating the root mean square aberration of the ST segment (ranging from 120 ms to 250 ms) with respect to the *acCELLerate* simulation. This was done for the six Wilson leads as well as for the three Einthoven leads for 20 setups representing different locations and transmural extents of the ischemic region (180 signals, results see Sect. 3.1).
After parametrization, the CA was used to run the study, where the left ventricular wall of all three datasets was divided using the 17-segment AHA scheme [3]. Hemispherical ischemic regions were placed at the center of each segment. Their radii, comprising both the CIZ and the BZ, varied from 5 mm to 25 mm for two of the anatomical models. The upper limit for the Visible Man dataset was set to 30 mm due to the thicker ventricular wall. 3 distinct series of simulations were carried out using different BZ radii: 2.8 mm, 4.8 mm and 9.6 mm. Simulations using the CA were conducted with a time step of 0.1 ms. The results were saved every 2 ms.

2.4. Forward-calculation

The TMVs from the simulations were interpolated on tetrahedral meshes of the respective anatomy to facilitate calculations with the finite element method. The bidomain model was used to calculate extracellular potentials on the body surface. It achieves a macroscopic treatment of intra- and extracellular space by taking into account the divergence of their respective current densities $\nabla(\sigma_e \nabla \Phi_e)$ and $\nabla(\sigma_i \nabla \Phi_i)$, which are assumed to compensate one another. This leads to an equation with the desired link between

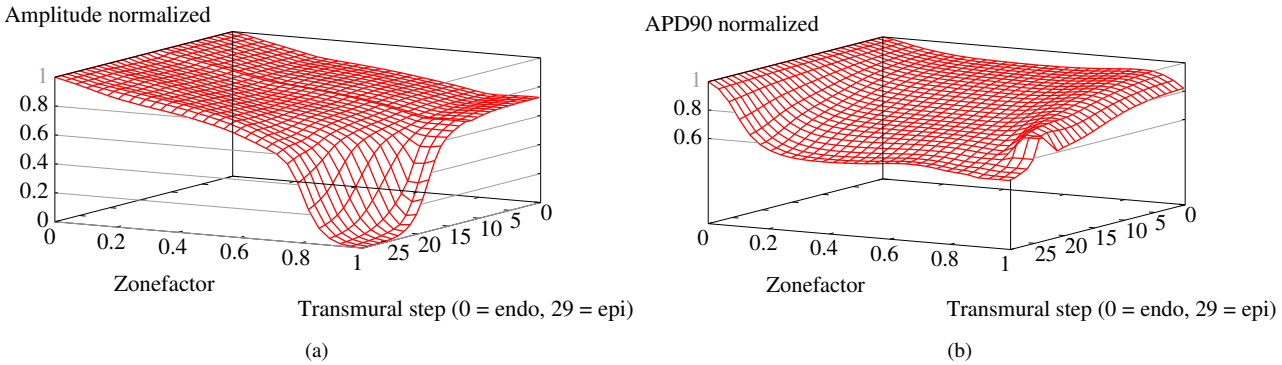

Figure 1. Dependency between the zone factor and the AP amplitude (a) as well as the APD_{90} (b) normalized to the physiological value in each transmural layer. AP amplitude and duration fall with increasing ZF. Incosistently with this finding, the algorithm considers diffused TMV courses to be APs in regions near the central ischemic zone and detects higher APD_{90}. Effects are most pronounced in subepicardial layers.

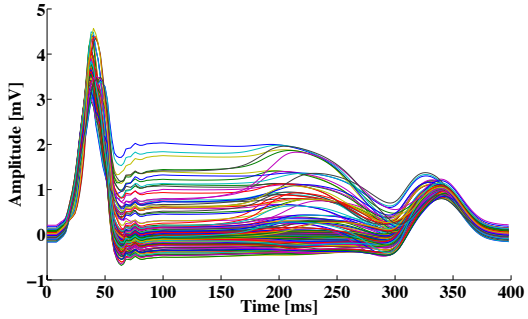

Figure 2. 238 Einthoven II signals for Patient D. Each signal belongs to a different combination of border zone and central ischemic zone radii.

TMVs V_m and extracellular potentials Φ_e, where the conductivity tensors σ_e and σ_i are set according to [9].

$$\nabla(\sigma_i \nabla V_m) = -\nabla((\sigma_i + \sigma_e)\nabla\Phi_e) \quad (1)$$

2.5. Finding optimum electrode positions

593 - 815 electrodes were equally distributed on each torso. Then, the ST deviation, defined as the absolute value of the sum of the 25 samples between 110 ms and 158 ms, was calculated for each possible set of 3 electrodes. To allow for a robust detection of ischemia under realistic noise conditions (noise amplitude 50 µV, SNR – 4.86 dB) within 100 heart beats and a maximum error rate of 0.1 %, the minimum ST deviation was set to 980 µV. Afterwards, 70 electrode positions which were able to detect the most ischemia setups for a single anatomical model were mapped onto the 2 other torsi and common statistics were obtained.

3. Results

3.1. Electrophysiological effects of ischemia

The RMV showed a nearly linear ascent from a physiological value of – 85 mV in healthy tissue to – 64 mV in the CIZ, not depending on the transmural location. Besides the increase of the RMV within the BZ, a decrease of the maximum TMV could be observed. Hence, the amplitude of the AP decreases significantly (Fig. 1 (a)). The effect varies transmurally and is most expressed in the epicardium. Each transmural course was normalized to its value in healthy tissue. The APD_{90} falls with increasing zonefactor (Fig. 1 (b)). The scheme is broken near the CIZ: here, the algorithm considers diffused TMV courses to be APs and detects higher APD_{90}. Because the CA is not able to model diffused currents, it was preferred to model low amplitude APs with short duration instead of just the RMV where diffused TMV courses are present in *acCELLerate*. The fourth electrophysiolgical parameter – the conduction velocity – showed a linear decline to 20% of the physiological value and no transmural variation.
The RMS deviation between the ST segment gained from CA and *acCELLerate* simulations was smaller than 0.02 mV for over 50% of the 180 extracted lead signals. 12 signals showed an aberration of more than 0.2 mV – mostly due to broadened QRS complexes ranging beyond 120 ms. Fig. 2 shows the Einthoven II signals for all 238 simulated ischemia setups of patient D.

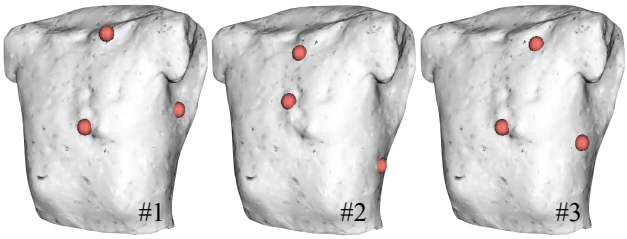

Figure 3. Optimum electrode positions determined considering all patient geometries. #1 is the optimum configuration for a border zone of 2.8 mm, #2 for one of 4.8 mm and #3 for 9.6 mm, respectively.

3.2. Optimum electrode positions

Electrode positions allowing for the detection of the highest number of ischemia setups showed inter-individual scattering. Table 1 shows the detection rates for optimum electrode positions regarding a single patient and the detection rates considering all patients using common electrode configurations shown in Fig. 3. Ischemia is harder to detect for patient VM than for the other two. The smaller the border zone and the greater the ischemic region, the easier the detection. Fig. 4 shows which fraction of ischemic setups could not be detected regarding the 17 AHA segments.

4. Discussion and conclusions

Results in Table 1 show a sensitivity of 49 - 60 %. In this study, the monitoring system was thus capable of detecting ischemic events almost as reliably as the 12-lead ECG in clinical studies, which produces typical sensitivities of 45 % [2] or 60.7 - 72.7 % [1]. The sensitivities in the two 12-lead studies, however, come with high specificity rates of 92 % and 94.9 - 97.1 %. Specificity rates cannot be produced in this study since they require a set of simulations that would represent the possible deviations within the physiological case. The rates can, however, be assumed to be in the same range, since the underlying mechanism of detecting ischemic events is the same and a strong correlation between the effects of physiological deviations in the heart beat and those of ischemia are not expected. The relatively good performance can therefore be attributed to

Table 1. Detection rates for ischemic regions with varying extent of border zone and total radius. Values in first lines were obtained using the best electrode configuration for each patient. For values in the second lines, common electrode configurations as shown in Fig. 3 were used.

	All radii				Radius >5 mm				Radius >10 mm				
	VM	K	D	∪	VM	K	D	∪	VM	K	D	∪	
BZ 2.8 mm	54 %	73 %	66 %		65 %	91 %	82 %		81 %	100 %	100 %		Individual
	48 %	73 %	61 %	60 %	58 %	91 %	76 %	77 %	76 %	90 %	100 %	88 %	Common
BZ 4.8 mm	51 %	71 %	64 %		61 %	88 %	79 %		76 %	100 %	100 %		Individual
	47 %	71 %	56 %	57 %	56 %	88 %	71 %	71 %	71 %	100 %	92 %	86 %	Common
BZ 9.6 mm	45 %	61 %	64 %		54 %	76 %	80 %		68 %	92 %	100 %		Individual
	38 %	61 %	48 %	49 %	46 %	76 %	60 %	60 %	57 %	92 %	78 %	74 %	Common

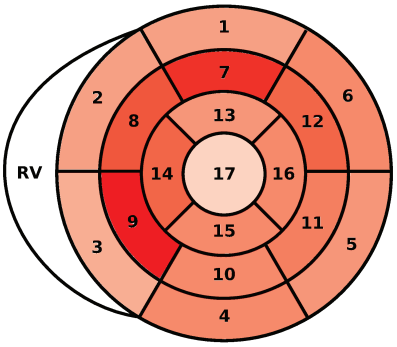

Figure 4. Detection rate using common electrode configurations with respect to the myocardial AHA segment. The darker the color, the more setups were not detected. The fraction of failed detections ranges from 23 % in the apex to 50 % in segment 9.

the optimized electrode positions and the imperfect nature of the models.

Fig. 4 shows that the location of the ischemia has small influence on its detectability. While electrode positions have been optimized to cover a large set of different radii, these positions seem to be particularly insensitive to ischemia of small radius. Future studies may focus on optimum positions for a detection of just the small radii.

4.1. Limitations

Due to the low number of patient models, the study is explicitly not meant to deliver a clinical guideline. It is rather a case study that shows the capability of simple wearable monitoring systems. Further tests on personalized models of an extended patient population are needed to justify a use of the electrode positions in a patient monitoring application. A comprehensive assessment of the modeling errors in addition to the measurement errors is required to quantify the overall statistical power of the study.

References

[1] Ornato JP, Menown IBA, Peberdy MA, Kontos MC, Riddell JW, Higgins GLr, et al. Body surface mapping vs 12-lead electrocardiography to detect ST-elevation myocardial infarction. Am J Emerg Med 2009;ISSN 0735-6757.

[2] Owens C, McClelland A, Walsh S, Smith B, Adgey J. Comparison of value of leads from body surface maps to 12-lead electrocardiogram for diagnosis of acute myocardial infarction. Am J Cardiol 2008;102:257–265.

[3] Cerqueira M, Weissman N, Dilsizian V, Jacobs A, Kaul S, Laskey W, et al. Standardized myocardial segmentation and nomenclature for tomographic imaging of the heart. Circulation 2001;105:539–542.

[4] Streeter DD. Handbook of Physiology: The Cardiovascular System. American Physiology Society, 1979; 61–112.

[5] Karl M, Seemann G, Sachse F, Dössel O, Heuveline V. Time and memory efficient implementation of the cardiac bidomain equations. In IFMBE Proceedings. 2008; .

[6] Keller DUJ, Weber FM, Seemann G, Dössel O. Ranking the influence of tissue conductivities on forward-calculated ecgs. IEEE Trans Biomed Eng 2010;57:1568–1576.

[7] ten Tusscher K, Panfilov A. Alternans and spiral breakup in a human ventricular tissue model. Am J Physiol Heart Circ Physiol 2006;291:H1088–100. ISSN 0363-6135.

[8] Weiss D, Ifland M, Sachse FB, Seemann G, Dössel O. Modeling of cardiac ischemia in human myocytes and tissue including spatiotemporal electrophysiological variations. Biomed Tech 2009;54:107–125.

[9] Gabriel S, Lau RW, Gabriel C. The dielectric properties of biological tissues: Ii. measurements in the frequency range 10 Hz to 20 GHz. Phys Med Biol 1996;41:2251–2269.

Address for correspondence:

Walther Schulze
Institute of Biomedical Engineering
Karlsruhe Institute of Technology (KIT)
Kaiserstr. 12, 76131 Karlsruhe, Germany
publications@ibt.kit.edu